Numerical comparison of two-dimensional Navier-Stokes flows on the whole plane and the periodic domain

Koji Ohkitani *
Research Institute for Mathematical Sciences, Kyoto University, Kyoto 606-8502, Japan

(Received 28 May 2023; accepted 1 December 2023; published 22 December 2023)

A majority of numerical experiments of the Navier-Stokes equations, lacking physical boundaries, have been conducted under periodic boundary conditions so far. In this paper, in order to access the effect of periodicity imposed upon the flow properties, we take up specifically two-dimensional incompressible flows and carry out numerical simulations on the whole plane to compare with those under periodic boundaries, with or without adjusting the Reynolds number. We solve the Navier-Stokes equations on a square domain using a finite-difference scheme to simulate flows on $\mathbb{R}^2$. After checking the time evolution of the Oseen vortex with the exact solution, we simulate merging of like-signed vortices to compare it with that under periodic boundaries. Generally speaking, we find that flows decay in norms faster on $\mathbb{T}^2$ than on $\mathbb{R}^2$, even when the Reynolds number is adjusted. We also simulate merging of three localized vortices that generates finer spatial structure in order to study the decay law of the total enstrophy and spatial patterns in vorticity. In this case, norms on $\mathbb{T}^2$ decay in a manner very close to how those on $\mathbb{R}^2$ do, but still marginally faster than those on $\mathbb{R}^2$. We also study the power law of the energy spectrum on $\mathbb{R}^2$, comparing it with the predictions of, for example, Gilbert's spiral model including $E(k) \sim k^{-11/3}$, which sits at the Sulem-Frisch borderline.

DOI: 10.1103/PhysRevFluids.8.124607

I. INTRODUCTION

Many works have been published in studying fundamental aspects of fluid turbulence numerically over the past nearly 50 years since the advent of so-called pseudospectral methods. They allow efficient numerical computations with exponential accuracy and, quite understandably, a majority of their implementations were conducted under periodic boundary conditions after expanding flow fields in Fourier series. Inevitably, the eigenvalues of the Stokes operator are discretized and have the lowest value away from zero, which corresponds to the existence of the fundamental periodic box. The flow fields in each box are affected by their periodic images via Poisson summation.

Also, in mathematical analysis of the Navier-Stokes equations, problems under periodic boundary conditions are easier to handle than those on the whole space. However, the precise relationship between the two is poorly understood and few papers discuss such matters.

In the case of three-dimensional (3D) turbulence there are works which study the domain size under the same boundary conditions, for example, [1,2]. For two-dimensional turbulence, the roles of boundary conditions and the domain shape were studied in [3]. Also, a relevant mathematical problem was investigated in [4]. A kind of transfer of regularity results was proved therein for the 3D Navier-Stoke equations: A $2L$-periodic solution on $\mathbb{T}^3$, which is smooth on a finite-time interval, converges to a smooth solution on the same time interval on $\mathbb{R}^3$ as $L \to \infty$. Conversely, if a solution

*ohkitani@kurims.kyoto-u.ac.jp

on $\mathbb{R}^3$ is smooth on a finite-time interval, then there exists a smooth periodic solution on the same time interval for a sufficiently long L.

In this paper, to consider the relationship between the two different kinds of boundary conditions, we take up the 2D Navier-Stokes equations of an incompressible fluid. We will focus on the forward cascade of enstrophy. Clearly the inverse energy cascade is affected by the presence of the lowest eigenvalue, that is, the eddies simply cannot grow larger than the size of the periodic box. While we will not study the energy inverse cascade directly, it is of interest to see how the forward enstrophy cascade is affected, because after all the transfer mechanisms of energy and enstrophy are just two different facets of the same triadic interaction in wave-number space.

We carry out numerical experiments on a large but finite square designed to mimic the whole plane $\mathbb{R}^2$. We then transfer the initial data onto the periodic domain $\mathbb{T}^2$ and carry out corresponding simulations in a parallel manner, with or without adjusting the Reynolds number on $\mathbb{T}^2$. Hence, when the Reynolds number is adjusted, any (qualitative) differences we observe should come from the effect of periodic images and/or the discretized wave-number modes associated with the lowest eigenvalue. We note that in [5] a systematic study was conducted to check the effect of periodic boundaries by increasing L in a spirit similar to [4]. However, we believe that the computations in periodic setting are fundamentally different from those conducted on the whole plane. Therefore, it is worth checking whether the existence of the low-wave-number cutoff actually yields a benign numerical artifact or something more serious. That is the rationale why we seek a direct comparison of flows on $\mathbb{R}^2$ and on $\mathbb{T}^2$.

The rest of this paper is organized as follows. In Sec. II we recall basic facts about the 2D Navier-Stokes equations and phenomenological theory of 2D turbulence. In Sec. III we describe numerical methods in some detail. In Sec. IV we present numerical results where we handle three different kinds of initial data, with or without adjusting the Reynolds number on $\mathbb{T}^2$. We begin by confirming an exact solution of the Oseen vortex as a validation of our approach and proceed to study the merger of two or three vortices. Section V is devoted to a summary and outlook.

II. FUNDAMENTALS

In term of vorticity ω the 2D incompressible Navier-Stokes equations read

$$\begin{aligned} \frac{\partial \omega}{\partial t} + \boldsymbol{u} \cdot \boldsymbol{\nabla} \omega &= \nu \triangle \omega, \\ \boldsymbol{\nabla} \cdot \boldsymbol{u} &= 0, \end{aligned} \tag{1}$$

where $\omega(\boldsymbol{x}, 0) = \omega_0(\boldsymbol{x})$ denotes the initial data, ν is the kinematic viscosity, $\boldsymbol{u} = -\boldsymbol{\nabla}^\perp \triangle^{-1} \omega$ is the incompressible velocity, and $\boldsymbol{\nabla}^\perp = (\partial_y, -\partial_x)$ is a skew derivative. We consider two different kinds of boundary conditions: on the whole plane $\omega(\boldsymbol{x}) \to 0$ as $|\boldsymbol{x}| \to \infty$ for $\boldsymbol{x} \in \mathbb{R}^2$ and on the periodic domain $\omega(\boldsymbol{x}) = \omega(\boldsymbol{x} + 2\pi \boldsymbol{n})$ for $\boldsymbol{x} \in \mathbb{T}^2$, where $\boldsymbol{n} = (n_1, n_2) \, \forall \, n_1, n_2 \in \mathbb{Z}$.

We recall scaling laws in phenomenological theory for a turbulent cascade in two dimensions, highlighting the differences stemming from the boundary conditions. We will consider a forward cascade of enstrophy in this paper. In homogeneous isotropic turbulence the following scaling laws are known (possibly with a logarithmic correction) for the energy spectrum $E(k)$ or alternatively for the enstrophy spectrum $Q(k) = k^2 E(k)$:

$$E(k) \sim \eta^{2/3} k^{-3}, \tag{2}$$

i.e., $Q(k) \sim \eta^{2/3} k^{-1}$, when k lies in the intermediate range (i.e., the inertial subrange), referred to as the Batchelor-Kraichnan-Leith (BKL) scaling [6–8]. Here $\eta(t) = -\frac{d}{dt} \langle \frac{\omega^2}{2} \rangle$ defines the dissipation rate of enstrophy per unit area, with angular brackets denoting the ensemble average for theory (or spatial averages for numerics).

TABLE I. Scaling of 2D turbulence.

Boundary conditions	Forward enstrophy cascade	Inverse energy cascade
Isotropic turbulence	$E(k) \sim \eta^{2/3} k^{-3}$	$E(k) \sim \epsilon^{2/3} k^{-5/3}$
Whole plane	$E(k) \sim (\eta')^{2/3} k^{-11/3}$	$E(k) \sim (\epsilon')^{2/3} k^{-7/3}$

As variants of Kolmogorov's relationship for 3D turbulence, we have

$$\langle \delta_\parallel u(r)[\delta\omega(r)]^2 \rangle = -2\eta r,$$

$$\langle [\delta_\parallel u(r)]^3 \rangle = \tfrac{3}{2}\epsilon r,$$

where $\delta_\parallel u(r)$ is the longitudinal velocity increment and $\delta\omega(r)$ the vorticity increment (see, e.g., [9]). They correspond to the Kolmogorov's 4/5 law in three dimensions.

By and large, the scaling law (2) has been verified by direct numerical simulations under periodic boundary conditions in many works, e.g., [10–12]. In contrast, for 2D turbulence on the whole plane we ought to consider the total enstrophy and its dissipation rate $\eta'(t)$. Accordingly, the scaling law would be altered, for k in the inertial subrange, as

$$E(k) \sim \eta'^{2/3} k^{-11/3}, \tag{3}$$

i.e., $Q(k) \sim \eta'^{2/3} k^{-5/3}$, where $\eta'(t) = -\frac{d}{dt}\int_{\mathbb{R}^2} \frac{\omega^2}{2} d\boldsymbol{x}$. This scaling law is related to the bound for the 2D Euler equations on $\mathbb{R}^2$, which will be referred to as the Sulem-Frisch (SF) scaling [13]. (N.B. The correct exponent $-11/3$ was given in the Appendix in [14].) It states the following: If $E(k) < Ck^{-s}$ for some $s > 11/3$, then $\Pi_{\rm ens}(k) \to 0$ as $k \to \infty$, where $\Pi_{\rm ens}(k)$ denotes the enstrophy spectral flux.

We recall that the scaling of the velocity structure function $\delta u(r) \sim r^a$ and that of the corresponding Fourier spectrum $E(k) \sim k^{-n}$ are related by $n = 2a + 1$ provided $1 < n < 3$ [15]. The scaling of homogeneous 2D turbulence $E(k) \sim k^{-3}$ is already on the borderline, with $\delta u(r) \sim r^1$. Thus, the scaling corresponding to $n = 11/3$ on the whole plane would be saturated and invisible on $\delta u(r)$; rather, it can appear on the vorticity increment $\delta\omega(r) \sim r^{1/3}$.

It is in order to recall some other phenomenological models for 2D turbulence. A model for a localized vorticity gradient where vorticity is distributed like the Heaviside step function was proposed in [16]. It predicts $E(k) \sim k^{-4}$ or equivalently $Q(k) \sim k^{-2}$.

In an attempt to interpolate between the BKL and the Saffman scaling laws, yet another model was proposed and examined in [17], where vorticity is assumed to be wound up around a coherent vortex. For a vortex with the azimuthal velocity $u_\theta \sim 1/r^{s-1}$, the spiral model predicts

$$E(k) \sim (\Gamma t)^{2/(s+1)} k^{-4+(s-1)/(s+1)},$$

where Γ denotes total circulation and s (>0) a real parameter. In particular, for a point vortex (i.e., $s = 2$) we have $E(k) \sim k^{-11/3}$, which coincides with the SF bound.[1] We summarize in Table I the scaling laws of 2D turbulence for both boundary conditions, in which power-law behaviors for inverse energy cascade are also included.

It is in order to comment on the possibility of anomalous dissipation of enstrophy, which has been studied both mathematically and numerically. In some class of weak solutions of the 2D Euler equations (see references cited for details), if vorticity is Hölder continuous $\delta\omega(r) \sim r^b$ for some $b > 0$, then enstrophy is conserved [18]. It is also conserved by any solution with finite

[1]This may be an accidental coincidence, because for the surface quasigeostrophic equation (i.e., with $s = 3$) we have $E(k) \sim k^{-7/2}$, whereas dimensional analysis based on the dissipation of $\int_{\mathbb{R}^2} \theta^2 d\boldsymbol{x}$ gives rise to a different scaling $E(k) \sim k^{-7/3}$.

total enstrophy [19,20]. According to the argument in [21], enstrophy is conserved in the limit of vanishing viscosity of 2D Navier-Stokes flows.

Incidentally, it is of interest to note that a system of three point vortices which collapses in finite time[2] *does* show anomalous dissipation of enstrophy [23]. Apparently, it is not known whether it is necessary to consider such a wild class of solutions as point vortices to realize a dissipation anomaly in two dimensions [18].

III. NUMERICAL METHODS

We will place numerical computations on $\mathbb{R}^2$ back to back with those on $\mathbb{T}^2$ by the following methods.

A. Whole plane $\mathbb{R}^2$

To simulate flows on $\mathbb{R}^2$ we use the simple method of domain truncation, which may be called the large box method (see [24]). Instead of $\mathbb{R}^2$, consider a square domain $[-L, L]^2$ of size $2L$, which is large in comparison with the characteristic length scale of the flow field in question. For $\boldsymbol{x} \in \mathbb{R}^2$, we solve (1), adopting a central finite-difference scheme. We use a fast Poisson solver for handling the Biot-Savart relationship to estimate the velocity.

Here the Dirichlet boundary conditions are imposed at the edges of the box as

$$\omega(x, \pm L) = \omega(\pm L, y) = 0, \quad -L \leqslant x, y \leqslant L,$$

because we handle well-localized vortices in a large box *without* the formation of boundary layers whose vorticity is essentially zero at the box boundaries. This approach seems plausible and can be checked *a posteriori* by watching vortices not close to the boundaries.[3]

Time marching is done by the fourth-order Runge-Kutta method with a typical time step $\Delta t = 5\times10^{-3}$. All the computations are done in double precision arithmetic. We refer the reader to Appendix A for details of the numerical schemes.

B. Periodic domain $\mathbb{T}^2$

For $\boldsymbol{x} \in \mathbb{T}^2$, we use a standard 2/3-dealiased Fourier pseudospectral method to solve (1). Time marching is done in the same way as on $\mathbb{R}^2$, that is, by the fourth-order Runge-Kutta method with $\Delta t = 5\times10^{-3}$. In order to compare 2D Navier-Stokes flows on the whole plane $\mathbb{R}^2$ with those on the 2D torus $\mathbb{T}^2 \equiv [-\pi, \pi]^2$, it is necessary to transcribe the initial data on the whole plane onto the periodic domain. We recall a method of transforming initial data from $\mathbb{T}^3$ to $\mathbb{R}^3$ was given in [4]. See also [27] for yet another example of such a construction.

Here we do something in the opposite direction, transforming the initial data on $\mathbb{R}^2$ to that on $\mathbb{T}^2$. We prepare initial conditions on $\mathbb{T}^2$ by periodizing those on $\mathbb{R}^2$ by assuming that they are well localized so that their boundary values are *de facto* zero (discussed below).

Assume we have a large square $[-L, L]^2$ with a size L (>0), which mimics $\mathbb{R}^2$. The size L is taken to be large in comparison with the scale of vortices.

We transform the spatial coordinates $\boldsymbol{x} \in \mathbb{R}^2$ to $\tilde{\boldsymbol{x}} \in \mathbb{T}^2$ by $\tilde{\boldsymbol{x}} = \frac{\pi}{L}\boldsymbol{x}$ and the vorticity by $\tilde{\omega} = K\omega$ for a constant K (>0). Hereafter, variables on $\mathbb{T}^2$ are denoted by a tilde. (In practice, numerically we use $[0, 2\pi]^2$ as the domain on $\mathbb{T}^2$.) Then the following obvious identity holds:

$$\int_{\mathbb{R}^2} \frac{\omega^2}{2} dx\, dy = \left(\frac{L}{\pi K}\right)^2 \int_{\mathbb{T}^2} \frac{\tilde{\omega}^2}{2} d\tilde{x}\, d\tilde{y}. \tag{4}$$

[2] A system of point vortices lies outside the standard scope of weak solutions because $\boldsymbol{u} \notin L^2_{\mathrm{loc}}$ [22].

[3] It is known that there are issues of assigning boundary conditions in vorticity on a bounded domain, when boundary layers of vorticity are formed. See, e.g., [25,26] for the issues.

We define the total enstrophy on $\mathbb{R}^2$ and the averaged enstrophy on $\mathbb{T}^2$ by

$$Q(t) \equiv \int_{\mathbb{R}^2} \frac{\omega^2}{2} dx\, dy,$$

$$q(t) \equiv \frac{1}{(2\pi)^2} \int_{\mathbb{T}^2} \frac{\tilde{\omega}^2}{2} d\tilde{x}\, d\tilde{y},$$

respectively. Then they are related by $Q(t) = (\frac{2L}{K})^2 q(t)$.

For later use, we also introduce the total palinstrophy $P(t)$ on $\mathbb{R}^2$ and the averaged palinstrophy $p(t)$ on $\mathbb{T}^2$ as

$$P(t) \equiv \int_{\mathbb{R}^2} \frac{|\nabla \omega|^2}{2} dx\, dy,$$

$$p(t) \equiv \frac{1}{(2\pi)^2} \int_{\mathbb{T}^2} \frac{|\nabla_{\tilde{x}} \tilde{\omega}|^2}{2} d\tilde{x}\, d\tilde{y},$$

where $\nabla_{\tilde{x}} = (\partial_{\tilde{x}}, \partial_{\tilde{y}})$. By the obvious identity

$$\int_{\mathbb{R}^2} \frac{|\nabla \omega|^2}{2} dx\, dy = \int_{\mathbb{T}^2} \frac{|\nabla_{\tilde{x}} \omega|^2}{2} d\tilde{x}\, d\tilde{y},$$

we have $P(t) = (\frac{2\pi}{K})^2 p(t)$.

The choice of K leaves room for arbitrariness, similar to the situations where some mathematical existence theorems deploy extensive norms, e.g., the Sobolev norm, and others intensive norms, e.g., the Hölder norm (see [28]). One way is to take $K = 1$ to keep pointwise vorticity unchanged, thereby leaving the local timescale, set by nonlinearity, unaffected. [In fact, this is also equivalent to having their averaged values matched $q(t) = \frac{1}{(2L)^2} Q(t)$.] Basically this option was adopted in [4,27]. To clarify the relationship between the transcription onto the periodic lattice and the Reynolds similarity, let us define the Reynolds number by

$$\mathrm{Re} = \frac{\int_{\mathbb{R}^2} |\omega(\boldsymbol{x})| d\boldsymbol{x}}{\nu}. \tag{5}$$

Under the transcription, the L^1-norm transforms as

$$\int_{\mathbb{R}^2} |\omega(\boldsymbol{x})| d\boldsymbol{x} = \left(\frac{L}{\pi}\right)^2 \frac{1}{K} \int_{\mathbb{T}^2} |\tilde{\omega}(\tilde{\boldsymbol{x}})| d\tilde{\boldsymbol{x}};$$

hence we have

$$\mathrm{Re} = \frac{\int_{\mathbb{T}^2} |\tilde{\omega}(\boldsymbol{x})| d\tilde{\boldsymbol{x}}}{\tilde{\nu}}, \tag{6}$$

where $\tilde{\nu} = (\frac{\pi}{L})^2 K \nu$ is the scaled viscosity. This means that we should modify the kinematic viscosity to $\tilde{\nu}$, to comply with the Reynolds similarity, that is, to keep the Reynolds number unchanged on $\mathbb{T}^2$.

If the kinematic viscosity is unchanged $\tilde{\nu} = \nu$, the Reynolds similarity holds only when we choose $K = (\frac{L}{\pi})^2$. For $K \neq (\frac{L}{\pi})^2$, we can still keep Re unchanged on $\mathbb{T}^2$ by modifying the value of the kinematic viscosity. We will take $K = 1$ throughout this paper and without loss of generality[4] we choose $K = 1$ and $\tilde{\nu} = (\frac{\pi}{L})^2 \nu$. Before presenting the numerical results, we emphasize that flows under periodic boundary conditions are affected by periodic images (through Poisson summation), while flows on the whole plane (i.e., a large box) are not. Our objective is to study the effects coming from their differences.

[4]When $K \neq 1$ we can obtain equivalent results on $\mathbb{T}^2$ by rescaling time as $\tilde{t} = K^{-1} t$.

TABLE II. Numerical parameters.

	Boundary conditions				
	Whole plane $\mathbb{R}^2$			Periodic domain $\mathbb{T}^2$	
Vorticity configuration	ν	L	N as in $[-N, N]^2$	K	Grid points
IC 1, Oseen vortex	2×10^{-2}	20	1024	1	2048^2
IC 2, two vortices	5×10^{-3}	20	1024	1	2048^2
IC 3, three vortices	2.5, 5×10^{-4}	40	2048	1	4096^2

IV. NUMERICAL RESULTS

A. Justification of domain truncation

We first double-check that the domain truncation method reproduces the Oseen vortex properly. Its initial condition (IC) is

$$\omega_0(r) = \frac{\Gamma}{\pi l^2}\exp\left(-\frac{r^2}{l^2}\right) \quad \text{(IC 1)},$$

where $r = |\boldsymbol{x}|$, $\Gamma = \int_{\mathbb{R}^2}\omega_0 d\boldsymbol{x}$ (=1, by definition) is velocity circulation, and l is the initial core radius. The 2D Navier-Stokes equations have the following decaying vortex as an exact solution:

$$\omega(r,t) = \frac{\Gamma}{\pi(4\nu t + l^2)}\exp\left(-\frac{r^2}{4\nu t + l^2}\right)$$

(see, e.g., [29,30]). As the solution is radial, that is, depends only on $r = |\boldsymbol{x}|$ in polar coordinates, the nonlinear term is identically annihilated $\boldsymbol{u}\cdot\nabla\omega \equiv 0$ and the Gaussian functional form emerges from the heat kernel.

It is readily verified that the corresponding azimuthal velocity is given by

$$u(r,t) = \frac{\Gamma}{2\pi r}\left[1 - \exp\left(-\frac{r^2}{4\nu t + l^2}\right)\right]$$

and the enstrophy of the Oseen vortex by

$$Q(t) = \frac{1}{2}\int_{\mathbb{R}^2}\omega(r,t)^2 dS = \frac{\Gamma^2}{4\pi(4\nu t + l^2)}.$$

On the other hand, its total kinetic energy is nonexistent, that is, divergent, as can be verified by

$$E(t) = \frac{1}{2}\int_0^R u(r,t)^2 2\pi\, r\, dr \sim \frac{\Gamma^2}{4\pi}\log R \to \infty \quad \text{as } R\to\infty.$$

Hence it cannot serve as a check of numerical calculations for inviscid fluids.

For the domain truncation we consider initial data whose core radius l is small compared with L, i.e., $l \ll L$. We use $\nu = 0.02$, $l = 2$, and $L = 20$ numerically. The numerical parameters are summarized in Table II, together with those for other initial data. We compare in Fig. 1 the numerically obtained $\omega(\boldsymbol{x}, t)$ for $\nu = 2\times10^{-2}$ on $\mathbb{R}^2$ with the exact solution, where excellent agreement is observed at several different times.

After transforming the initial data to $\mathbb{T}^2$ by the method described above with $K = 1$, we solve the 2D Navier-Stokes equations in vorticity form (1) on $\mathbb{T}^2$, with or without adjusting the Reynolds number. In this case of a linear problem, the choice of K is actually insignificant. Because the boundary values are extremely small $\omega_0(L) = \exp[-(L/l)^2]/4\pi = e^{-100}/4\pi \approx 3.0\times10^{-45}$, they do not conflict with periodic boundaries in practice. (Similar remarks hold true for IC 2 and 3 below.)

In Fig. 2 we show the time evolution of enstrophy, normalized by the initial values $Q(0) = 1/16\pi \approx 0.02$ and $q(0) = Q(0)/(2L)^2 = 1.25\times10^{-5}$. For the Oseen vortex we again confirm that

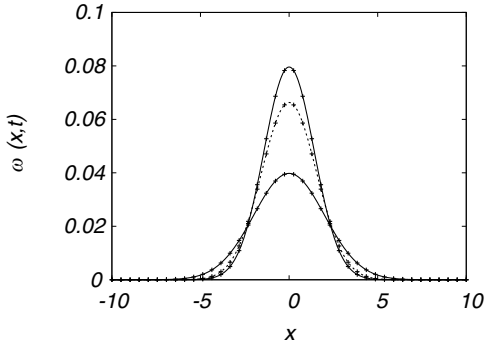

FIG. 1. Comparison of time evolution of IC 1: the Oseen vortex, numerical results (curves), and exact solutions (symbols). Time runs from top to bottom: $t = 0$, 10, and 50.

the numerical result agrees with the exact solution. For the periodic case enstrophy decays a bit faster, when the Reynolds number is adjusted using scaled $\tilde{\nu} = (\pi/L)^2\nu$. A slight difference is appreciable, which is due to the difference in boundary conditions, that is, the effect of the Poisson summation of periodic images. On the other hand, when the Reynolds number is not adjusted, using ν as is, the decay takes place much faster, actually exponentially in time (confirmed in the inset). We conclude that domain truncation works fine for handling the 2D Navier-Stokes flows on the whole plane. We also note that the periodic version of heat solutions in 2D is given by a two-dimensional θ function (see Appendix B).

B. Merger of two vortices

To see how the flow fields are affected by the difference in the boundary conditions further, we next consider a simple configuration of two vortices of the same sign. For the experiment on the whole plane, we take the initial data as

$$\omega_0(\boldsymbol{x}) = \exp\left(-\frac{(x+a)^2+y^2}{l^2}\right) + \exp\left(-\frac{(x-a)^2+y^2}{l^2}\right) \quad \text{(IC 2)},$$

where $a = 5$, $l = 2$, and $\nu = 5\times10^{-3}$.

For the calculation on the whole plane $\mathbb{R}^2$, we use $L = 20$ and $N = 1024$ for a grid $[-N, N]^2$. For the calculation on the periodic domain $\mathbb{T}^2$, we use accordingly 2048^2 grid points, with $K = 1$.

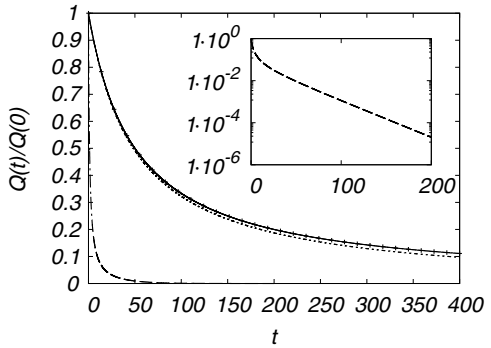

FIG. 2. Plot of normalized enstrophy of IC 1: the Oseen vortex, $Q(t)/Q(0)$ on $\mathbb{R}^2$ (solid curve), $q(t)/q(0)$ with $\tilde{\nu}$ on $\mathbb{T}^2$ (dotted curve), and $q(t)/q(0)$ with ν on $\mathbb{T}^2$ (dashed curve). The inset shows a semilogarithmic plot of the last quantity. Also plotted is the analytical result $Q(t)/Q(0) = \frac{1}{\nu t+1}$ (pluses).

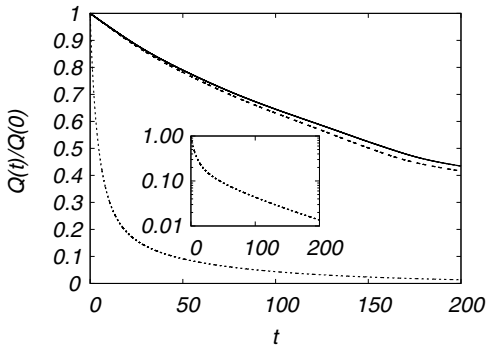

FIG. 3. Evolution of normalized enstrophy of IC 2 for two merging vortices: $Q(t)/Q(0)$ on $\mathbb{R}^2$ (solid curve), $q(t)/q(0)$ with $\tilde{\nu}$ on $\mathbb{T}^2$ (dashed curve), and $q(t)/q(0)$ with ν on $\mathbb{T}^2$ (dotted curve). The inset shows a semilogarithmic plot of the last quantity.

In Fig. 3 we show the time evolution of enstrophy $Q(t)$ on $\mathbb{R}^2$ and that of $q(t)$ on $\mathbb{T}^2$ for unscaled $\nu = 5\times10^{-3}$ and scaled $\tilde{\nu} = (\frac{\pi}{L})^2\nu$. They are normalized by initial values $Q(0) = 6.28$ and $q(0) = 3.80\times10^{-3}$, respectively. With scaled $\tilde{\nu}$, the enstrophy decays a bit faster on $\mathbb{T}^2$ than on $\mathbb{R}^2$. With unscaled ν, the enstrophy decay is much faster on $\mathbb{T}^2$, actually exponentially in time, as confirmed in the inset. These features are qualitatively the same as in the case of the Oseen vortex.

On $\mathbb{T}^2$ the Poincaré inequality is available because of the presence of the smallest eigenvalue of the Stokes operator, the simplest of which reads $\|\phi\|_{L^2} \leqslant C\|\nabla\phi\|_{L^2}$ for $\exists C$ (>0) for any $\phi(\boldsymbol{x})$ (see, e.g., [31,32]). As a result an exponential decay is obtained as an upper bound. This is not the case on $\mathbb{R}^2$ and for $\boldsymbol{u}_0 \in L^2(\mathbb{R}^2)$ we have instead [33,34] $\|\nabla\boldsymbol{u}\|_{L^2} \leqslant Ct^{-1/2}$, with a constant C, that is, $Q(t) \leqslant C^2/2t$. The numerical results above are consistent with the analysis, as can be verified by plotting $(\nu t + 1)Q(t)$ (figure omitted).

In Fig. 4 we show vorticity contours on $\mathbb{R}^2$ at several different times. We note that it takes a long time $t \approx 200$ to complete the merging process. As for the results on the periodic domain, we

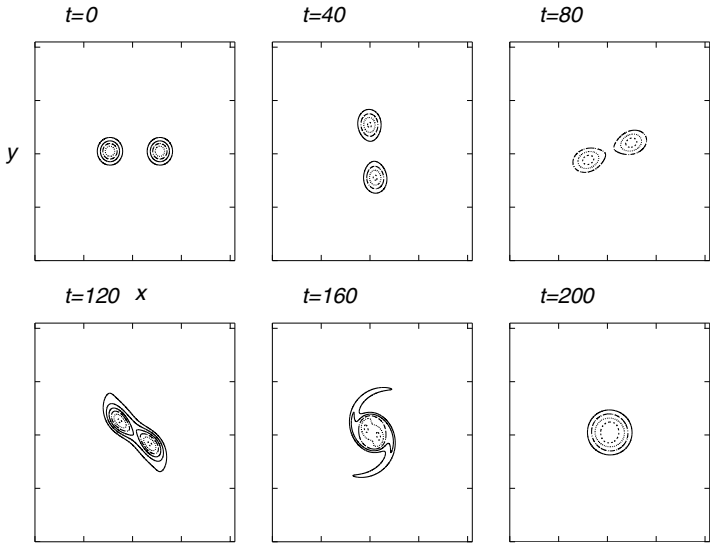

FIG. 4. Time evolution of vorticity contours on $\mathbb{R}^2$ for IC 2. Six levels of contours are drawn between the maximum and minimum of $\omega(x, y)$ on $[-L, L]^2$ with $L = 20$.

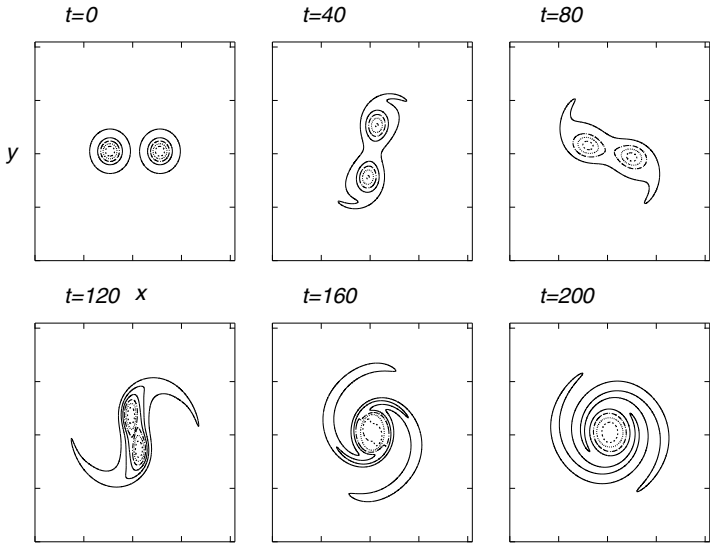

FIG. 5. Time evolution of vorticity contours on $\mathbb{T}^2$ for IC 2, with the Reynolds number adjusted using scaled $\tilde{\nu}$. Six levels of contours are drawn between the maximum and minimum of $\tilde{\omega}(x, y)$ on $[-\pi, \pi]^2$.

show vorticity contours on $\mathbb{T}^2$ at several different times using $K = 1$, with scaled $\tilde{\nu}$ in Fig. 5 and with unscaled ν in Fig. 6. When we adjust the Reynolds number, we observe a similarity in contour patterns in Figs. 4 and 5, while they are not exactly the same. In Fig. 6 we notice that with unscaled ν it takes a shorter time $t \approx 100$ to the complete merging process, consistent with the much faster decay.

As for the spectral properties, it turns out that the enstrophy spectra have excitations restricted in the lower-wave-number range, with no power-law behavior observed. We refrain from describing their details further.

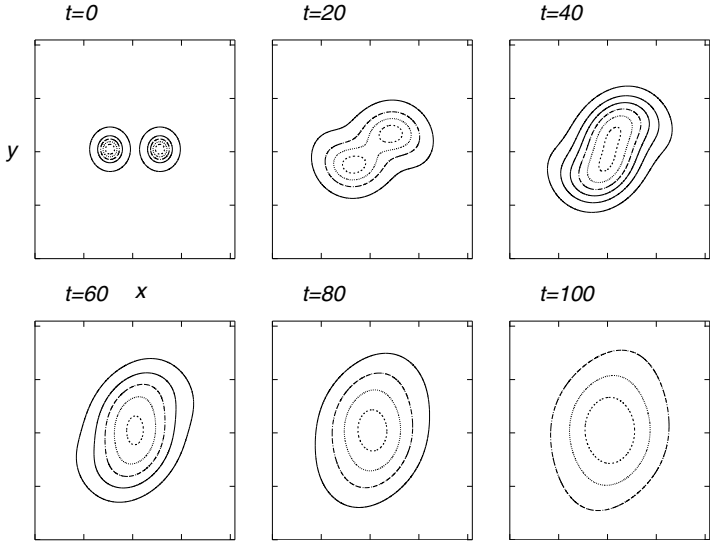

FIG. 6. Time evolution of vorticity contours on $\mathbb{T}^2$ for IC 2 using unscaled ν without adjusting the Reynolds number. Six levels of contours are drawn between the maximum and minimum of $\tilde{\omega}(x, y)$ on $[-\pi, \pi]^2$.

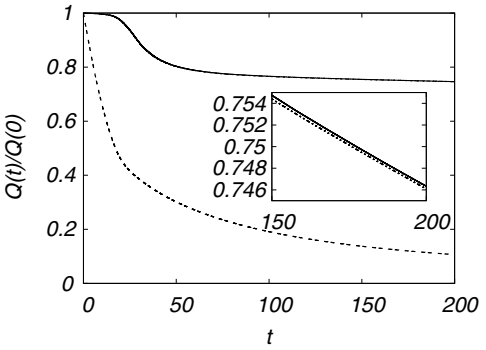

FIG. 7. Time evolution of normalized enstrophy for IC 3: $Q(t)/Q(0)$ on $\mathbb{R}^2$ with $\nu = 2.5\times10^{-4}$ (solid curve) and $q(t)/q(0)$ on $\mathbb{T}^2$ with $\tilde{\nu} = \nu(\pi/L)^2$ (dotted curve) and with $\nu =$ (dashed curve). The inset shows a close-up view of the former two.

C. Merging of three localized vortices

As noted above, the numerical experiments of merging two vortices turn out to be governed by nearly linear dynamics. In this section we seek another initial datum that generates a structure with finer spatial scales as we are interested in the scaling of 2D turbulence. To this end, following [35], we consider the collision of three point vortices at a point [36,37] and adapt it to the numerical simulations. The initial condition is obtained by regularization with a Gaussian filter.

Consider a system of three point vortices. Under stringent conditions on the strength of vortices and their initial locations, they can be set to collapse at a point in finite time in a self-similar manner (see Appendix C).[5] An example of such an initial condition is a set of point vortices of strengths π, π, and $-\pi/2$ located at $(-5, 0)$, (5,0), and $(5, 5\sqrt{2})$, respectively. The initial condition is a regularized version of such a system, that is,

$$\omega_0(\boldsymbol{x}) = \pi \exp\left(-\frac{(x-5)^2+y^2}{l^2}\right) + \pi \exp\left(-\frac{(x+5)^2+y^2}{l^2}\right) - \frac{\pi}{2}\exp\left(-\frac{(x-5)^2+(y-5\sqrt{2})^2}{l^2}\right) \quad \text{(IC 3)},$$

where $l = 2$.

To compare with our initial setting, IC 3, after rescaling with $\alpha = \pi/2$ and $\beta = 5$ in Appendix C, we have

$$t = \frac{\beta^2}{\alpha}t' = 3\sqrt{2}\pi\frac{5^2}{\pi/2} = 150\sqrt{2} \approx 210,$$

as a rough estimate of collapse of three vortices. Needless to say, because of regularization of the initial data and the presence of dissipativity, we would expect merging rather than a hard collapse.

We carry out simulations with lower viscosity and check the effect of the finite size of the box. We consider the cases $\nu = 2.5$ and 5×10^{-4} with $L = 40$ and $N = 2048$ on $\mathbb{R}^2$. On $\mathbb{T}^2$, we compute on a 4096^2 grid using $K = 1$, with or without adjusting the Reynolds number.

In Fig. 7 we show the evolution of the enstrophy on $\mathbb{R}^2$ and on $\mathbb{T}^2$, with unscaled $\nu = 2.5\times10^{-4}$ and scaled $\tilde{\nu} = \nu(\pi/L)^2$. They are normalized by the initial values $Q(0) = 69.7$ and $q(0) = 1.08\times10^{-2}$. When the Reynolds number is adjusted, the enstrophy decay is remarkably

[5]Strictly speaking, this form of solution remains valid only on $\mathbb{R}^2$ as the system of equations of point vortices is modified on $\mathbb{T}^2$ (see, e.g., [38,39]). The existence of collapsing (and expanding) solutions on $\mathbb{T}^2$ was proved in [38].

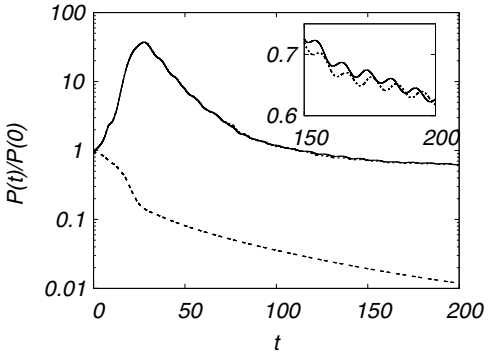

FIG. 8. Semilogarithmic plot of normalized palinstrophy for IC 3: $P(t)/P(0)$ on $\mathbb{R}^2$ with $\nu = 2.5\times10^{-4}$ (solid curve) and $p(t)/p(0)$ on $\mathbb{T}^2$ with $\tilde{\nu} = \nu(\pi/L)^2$ (dotted curve) and with ν (dashed curve). The inset shows a close-up linear plot of the former two.

close for both boundary conditions, to the extent that they are virtually indistinguishable in the main plot. However, in the magnified inset we do observe a marginally faster decay on $\mathbb{T}^2$ than on $\mathbb{R}^2$. [The same feature is also observed with $\nu = 5\times10^{-4}$ and $\tilde{\nu} = \nu(\pi/L)^2$ (figure omitted).] On the other hand, if the Reynolds number is not adjusted, that is, with unscaled ν, the decay on $\mathbb{T}^2$ takes place much faster.

In Fig. 8 we compare the evolutions of the palinstrophies, which are normalized by initial values $P(0) = 35.0$ and $p(0) = 0.888$. We observe prominent peaks in their growth on $\mathbb{R}^2$ and $\mathbb{T}^2$ with the Reynolds number adjusted using scaled $\tilde{\nu}$ and even at the late stage they virtually collapse on

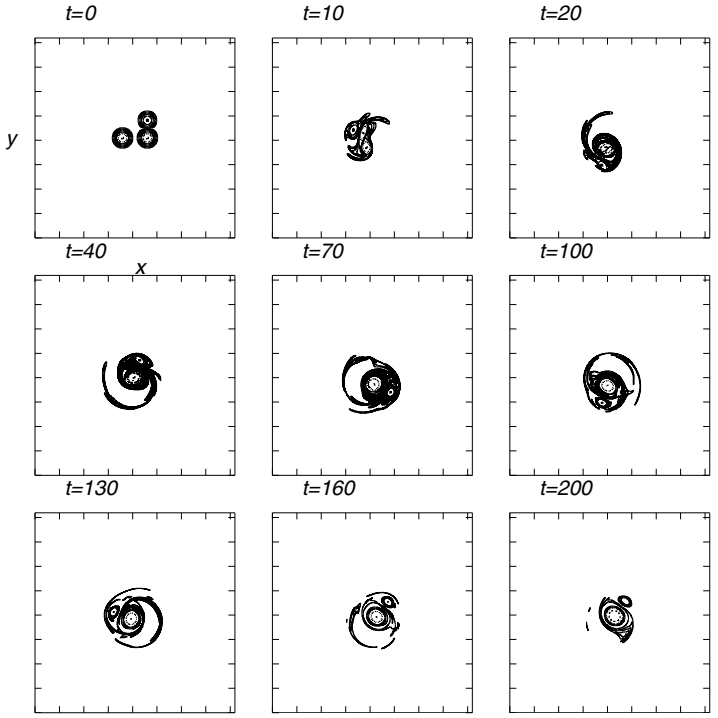

FIG. 9. Evolution of vorticity contours for IC 3 with $\nu = 2.5\times10^{-4}$, on $[-L, L]^2 \subset \mathbb{R}^2$ ($L = 40$), using thresholds $\omega = 3, \pm3/2^n$ ($n = 1, \ldots, 6$).

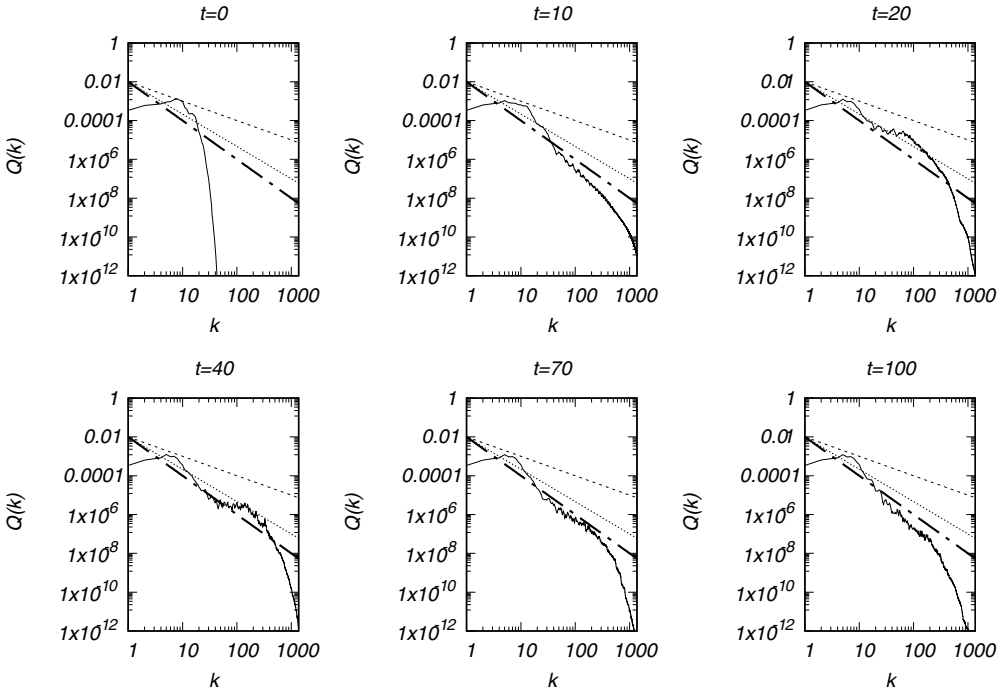

FIG. 10. Enstrophy spectrum $Q(k)$ for IC 3 on $\mathbb{R}^2$ at different times. The straight lines are the guide for the BKL -1 (dashed curves), SF $-5/3$ (dotted curves), and Saffman -2 (dash-dotted curves) slopes.

each other. In the inset we show a close-up view of their linear plots, where we observe that decay takes place with oscillations and marginally faster on $\mathbb{T}^2$ than on $\mathbb{R}^2$. Finally, with unscaled ν, i.e., without adjustment of the Reynolds number, the palinstrophy decays straight away without showing an initial increase.

In Fig. 9 we plot vorticity contours on $\mathbb{R}^2$ for $\nu = 2.5\times10^{-4}$ at several different times. We can see filaments with fine scales trailing behind the vortices up to $t \approx 200$. To check that the result is robust, we confirm the agreement with a computation using the parameters $L = 20$ and $N = 2048$, thereby halving the mesh size (figure omitted). In order to characterize how small scales are excited,

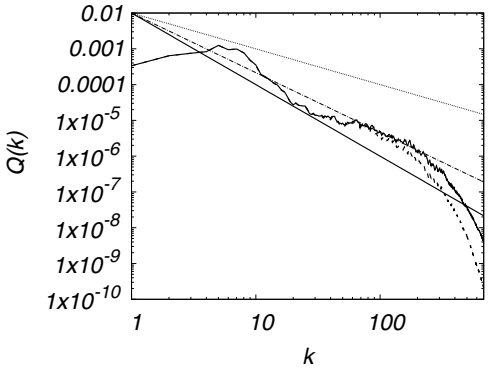

FIG. 11. Enstrophy spectrum $Q(k)$ for IC 3 averaged over $t = 20, \ldots, 50$, on $\mathbb{R}^2$ for $\nu = 2.5\times10^{-4}$ (solid curve), $\nu = 5\times10^{-4}$ (dashed curve), and guide slopes -1, $-5/3$, and -2 from above. The exponent looks close to -1.

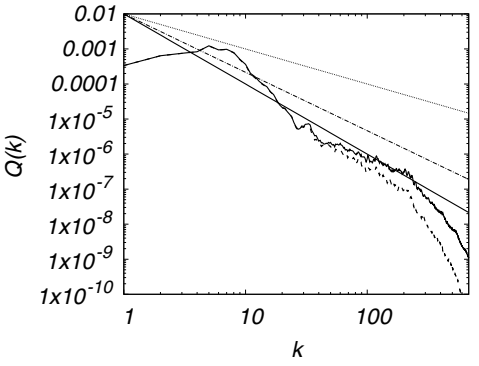

FIG. 12. Enstrophy spectrum $Q(k)$ for IC 3 averaged over $t = 50, \ldots, 80$, on $\mathbb{R}^2$ for $\nu = 2.5\times10^{-4}$ (solid curve) $\nu = 5\times10^{-4}$ (dashed curve), and guide slopes -1, $-5/3$, and -2 from above. The exponent looks close to $-5/3$.

we introduce the Fourier power spectrum of enstrophy. Using the domain truncation method for well-localized vortices, a surrogate for a Fourier integral is to consider a Fourier series assuming a long periodicity. Numerically, we define the enstrophy spectrum $Q(k)$, on both $\mathbb{T}^2$ and $\mathbb{R}^2$, as

$$Q(k) = \frac{1}{2} \sum_{k \leqslant |\boldsymbol{k}| < k+1} |\hat{\omega}(\boldsymbol{k}, t)|^2,$$

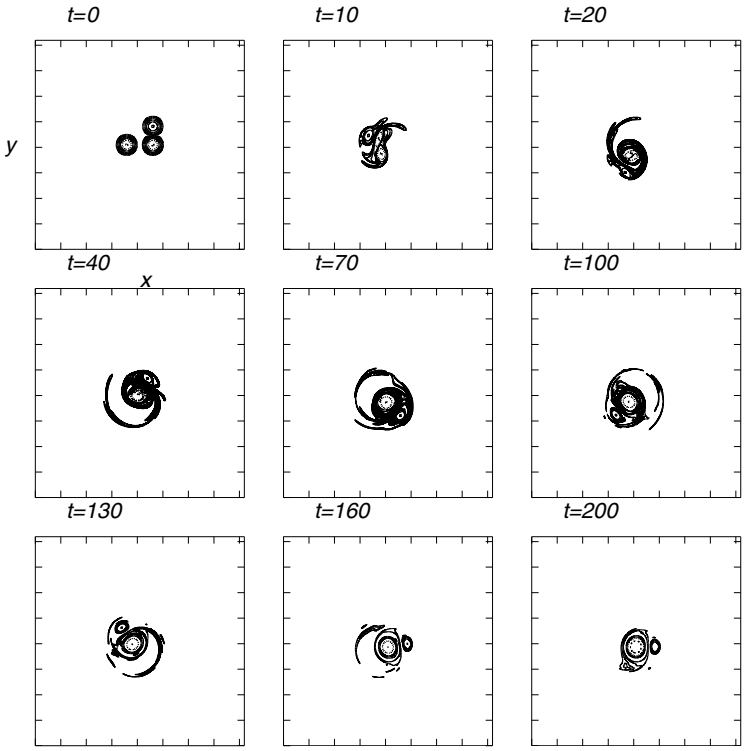

FIG. 13. Evolution of vorticity contours for IC 3, with scaled $\tilde{\nu}$ on $[-\pi, \pi]^2 \subset \mathbb{T}^2$, using thresholds $\tilde{\omega} = 3, \pm 3/2^n$ $(n = 1, \ldots, 6)$.

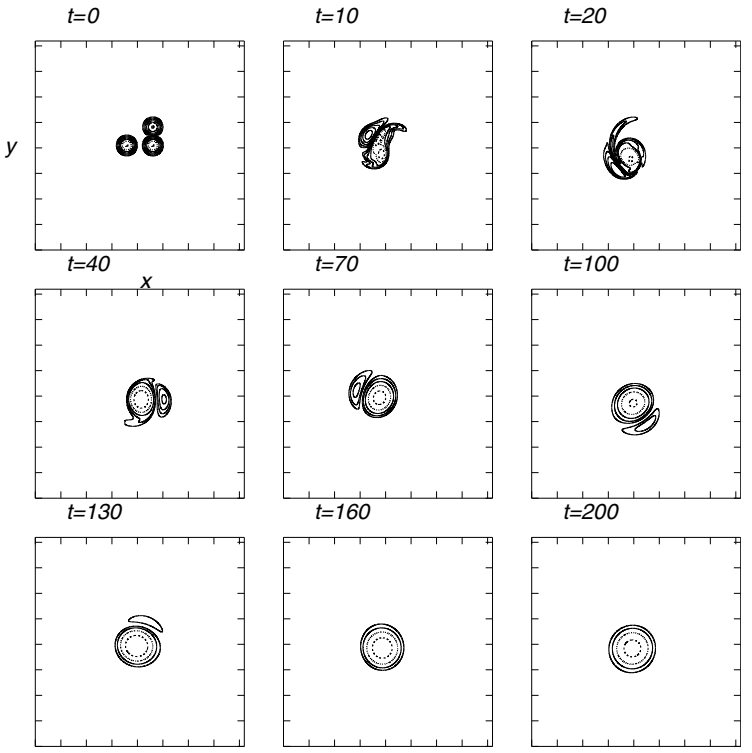

FIG. 14. Evolution of vorticity contours for IC 3 on $[-\pi,\pi]^2 \subset \mathbb{T}^2$, using ν without adjusting the Reynolds number. The thresholds are $\tilde{\omega} = 3, \pm 3/2^n$ $(n = 1, \ldots, 6)$.

where the Fourier coefficient $\hat{\omega}(\boldsymbol{k}, t)$ is defined as

$$\omega(\boldsymbol{x}, t) = \sum_{\boldsymbol{k}} \hat{\omega}(\boldsymbol{k}, t) e^{i\boldsymbol{k}\cdot\boldsymbol{x}}.$$

To Fourier analyze data on $\mathbb{R}^2$, we simply define $\tilde{\omega}(\boldsymbol{x}) = \omega(\boldsymbol{x})$ at each time in the definition in Sec. III A, since we are interested only in the scaling.

In Fig. 10 we show the enstrophy spectrum for $\nu = 2.5\times10^{-4}$ at different times along with three guide slopes -1 (BKL), $-5/3$ (SF), and -2 (Saffman). Particularly in the early stage $t < 70$, a power-law behavior is seen, although it has sizable fluctuations.

To suppress the fluctuations we take local time averages of $Q(k)$ and study the averaged spectrum. In Fig. 11 we show the spectrum averaged over $20 \leqslant t \leqslant 50$, and the power-law appears to be close to -1 (the BKL value). In Fig. 12 we show the average over $50 \leqslant t \leqslant 80$, which shows a bit steeper slope closer to $-5/3$. Because of the limited-wave-number range, we refrain from determining the slope precisely, but the exponent lies somewhere between -1 and $-5/3$ in the early stage of development. The latter exponent is to be compared with Gilbert's spiral model as we observe trailing filaments wound up around the central region. Next we consider the case of a periodic domain. When the Reynolds number is adjusted with the use of scaled kinematic viscosity $\tilde{\nu}$, we observe in Fig. 13 that vorticity contours on $\mathbb{T}^2$ are close to those on $\mathbb{R}^2$ in Fig. 9. Careful observation reveals that for $t \geqslant 130$ the vortices go around with their phase offset from those on $\mathbb{R}^2$. We also studied the enstrophy spectra, but again they are close to the ones on $\mathbb{R}^2$ (figure omitted). In Fig. 14 we show vorticity contours on $\mathbb{T}^2$ computed using ν without Reynolds number adjustment. Already at $t = 100$ a well-defined vortex emerges which is accompanied by a remnant of filaments.

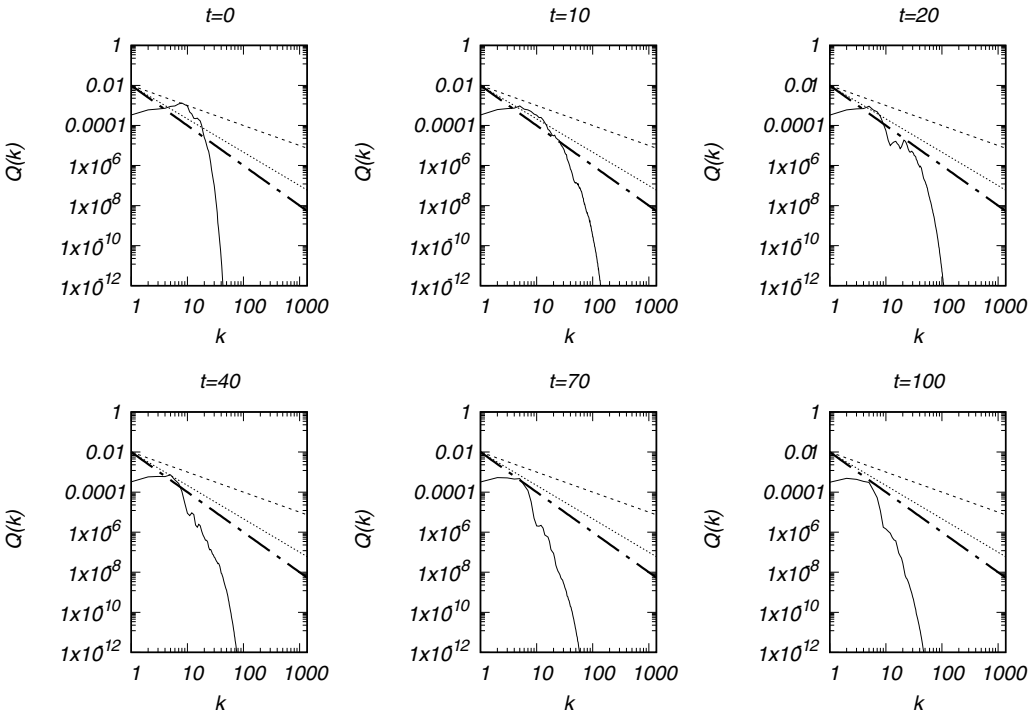

FIG. 15. Enstrophy spectrum $Q(k)$ for IC 3 on $\mathbb{T}^2$ at different times, using ν without adjusting the Reynolds number.

Accordingly, the enstrophy spectra in Fig. 15 show a rapid decay in k with no sign of power-law behavior, which is consistent with the faster decay of enstrophy.

V. SUMMARY AND OUTLOOK

We have formalized numerical methods that can handle flows on $\mathbb{R}^2$ and put them into practice. On one hand, we computed well-localized flows in a large box by domain truncation, with zero Dirichlet boundary conditions. On the other hand, we computed them on a periodic lattice after copying them with or without adjusting the Reynolds number. It should be stressed that the latter is affected by periodic images (through Poisson summation), while the former is not.

In comparative experiments of the vortex merger, we found that merging takes place faster on $\mathbb{T}^2$ than on $\mathbb{R}^2$, to the effect that the former decays a bit more quickly even when the Reynolds number is adjusted on $\mathbb{T}^2$.

We also simulated the collapse of three vortices, which leads to the generation of finer scales. When the Reynolds number is adjusted, their decay in norms is remarkably close for both boundary conditions. Nonetheless, the decay is marginally faster on $\mathbb{T}^2$ than on $\mathbb{R}^2$. It is not known why they are very close to each other in the IC 3 case of higher Reynolds numbers.

In physically oriented journals, numeral simulations under periodic boundaries, e.g., by pseudospectral methods, have frequently been reported. Caveats are often cast regarding usage of periodic flows for studying more realistic flows. The present results lend support for that at least partially, so long as flow fields are spatially well localized. This also supports a view that nonlocal interaction in the Navier-Stokes equations is not strong, e.g., "what happens to a given fluid element is only weakly affected by distant fluid elements (through the pressure term)" [28].

In these cases of significant nonlinear effects, we observed a power-law scaling of turbulence $Q(k) \sim k^{-n}$ for some exponent n. While the exponents remain inconclusive due to fluctuations, they lie in $1 \leqslant n \leqslant 2$. It is of interest to note that $Q(k) \sim k^{-5/3}$, i.e., $E(k) \sim k^{-11/3}$, appears in Gilbert's spiral model due to a point vortex. It also coincides with the SF borderline, beyond which the enstrophy cascade is no longer sustainable on $\mathbb{R}^2$.

The very late stage of evolution of 2D Navier-Stokes flows under periodic boundaries are well described by periodic heat solutions, that is, Riemann θ functions. The method of a self-similar profile that works fine on $\mathbb{R}^2$ would not work on $\mathbb{T}^2$, at least as it is. This is because the governing equations for self-similar solutions are at variance with spatial periodicity. It is of interest to see if and how we may characterize local self-similarity on $\mathbb{T}^2$.

It is left to future work to study the scaling with ever smaller values of viscosity, hopefully addressing the possibility of a dissipation anomaly on the whole plane. Also of interest is to compute 3D Navier-Stokes flows on $\mathbb{R}^3$ and compare them with those on $\mathbb{T}^3$.

ACKNOWLEDGMENTS

This work was supported by the Research Institute for Mathematical Sciences, an International Joint Usage/Research Center located at Kyoto University. This work was also supported by JSPS KAKENHI Grant No. JP21K20322. The author is grateful to reviewers' comments, particularly on the Reynolds similarity.

APPENDIX A: NUMERICAL SCHEME

We give a brief description of the finite-difference scheme for handling (1) numerically on the whole plane.

Consider a discretization of the vorticity (for $i, j = -N, \ldots, N$ hereafter) $\omega_{i,j} = \omega(x_i, y_j)$, where $x_i = hi$ and $y_j = hj$. Here $h = \frac{L}{N}$ is a spatial mesh for the size $2L$ and the number of grid points is $(2N+1)^2$.

We then discretize the advection term as

$$\boldsymbol{u} \cdot \nabla \omega(x_i, y_j) = u_{i,j} \frac{\omega_{i+1,j} - \omega_{i-1,j}}{2h} + v_{i,j} \frac{\omega_{i,j+1} - \omega_{i,j-1}}{2h},$$

where the velocity is given by

$$u_{i,j} = \frac{\psi_{i,j+1} - \psi_{i,j-1}}{2h}, \quad v_{i,j} = -\frac{\psi_{i+1,j} - \psi_{i-1,j}}{2h}.$$

The stream function is given $\psi_{i,j} = -\triangle^{-1}\omega_{i,j}$ by inverting the Laplacian via the Poisson solver under zero Dirichlet boundary conditions $\omega_{i,\pm N} = \omega_{\pm N,j} = 0$ $(-N \leqslant i, j \leqslant N)$ at the box edges. Also, the dissipative term is discretized as

$$\triangle \omega(x_i, y_j) = \frac{\omega_{i+1,j} - 2\omega_{i,j} + \omega_{i-1,j}}{h^2} + \frac{\omega_{i,j+1} - 2\omega_{i,j} + \omega_{i,j-1}}{h^2}.$$

APPENDIX B: POISSON SUMMATION FORMULA FOR HEAT SOLUTIONS

We recall formulas for heat solutions on $\mathbb{T}^n = \mathbb{R}^2/(2\pi\mathbb{Z})^n, n \in \mathbb{Z}$. Consider, for simplicity, $\frac{\partial u}{\partial t} = \triangle u$, where $u = u(\boldsymbol{x}, t), \boldsymbol{x} \in \mathbb{T}^n$.

The Poisson summation formula states (see, e.g., [40])

$$u = \frac{1}{(4\pi t)^{n/2}} \sum_{\boldsymbol{l}} \exp\left(-\frac{|\boldsymbol{x} + 2\pi \boldsymbol{l}|^2}{4t}\right) = \frac{1}{(2\pi)^n} \sum_{\boldsymbol{k}} \exp[-t|\boldsymbol{k}|^2 + i(\boldsymbol{k}, \boldsymbol{x})],$$

where $\boldsymbol{k} = (k_1, k_2, \ldots, k_n)$, $\boldsymbol{l} = (l_1, l_2, \ldots, l_n)$, and $(\boldsymbol{l}, \boldsymbol{x})$ is an inner product. When $n = 1$ we have $u = \frac{1}{\pi}\theta_3(x, \frac{4it}{\pi})$, because

$$u = \frac{1}{\sqrt{4\pi t}} \sum_l \exp\left(-\frac{|x + \pi l|^2}{4t}\right) = \frac{1}{\pi} \sum_k \exp(-4k^2 t + 2ikx),$$

where θ_3 denotes one of the conventional (π-periodic) elliptic theta functions

$$\theta_3(x, it) = \frac{1}{\pi} \sum_l \exp\left(-\frac{|x + \pi l|^2}{\pi t}\right)$$

[41,42]. For $n \geqslant 2$ multidimensional Riemann θ functions are defined by [41]

$$\theta(x_1, x_2, \ldots, x_n) = \sum_{\boldsymbol{k}} \exp[2\pi i(\boldsymbol{x}, \boldsymbol{k}) - (\boldsymbol{k}, \boldsymbol{T}\boldsymbol{k})],$$

where $\boldsymbol{T}$ denotes an $n \times n$ symmetric matrix with a positive-definite real part. In particular, when $n = 2$ we have

$$u = \frac{1}{4\pi t} \sum_{\boldsymbol{l}} \exp\left(-\frac{|\boldsymbol{x} + 2\pi \boldsymbol{l}|^2}{4t}\right) = \frac{1}{(2\pi)^2} \sum_{\boldsymbol{k}} \exp[-t|\boldsymbol{k}|^2 + 2\pi i(\boldsymbol{k}, \boldsymbol{x})].$$

The right-hand side can be written $\frac{1}{(2\pi)^2}\theta(\frac{x_1}{2\pi}, \frac{x_2}{2\pi})$, where $\boldsymbol{T} = t\boldsymbol{I}$, with $\boldsymbol{I}$ an identity matrix.

APPENDIX C: COLLAPSE OF THREE POINT VORTICES

For convenience, we recall a well-known result (see [36,37]). Consider a set of three point vortices of strength $(\kappa_1, \kappa_2, \kappa_3) = (2, 2, -1)$ located initially at $\boldsymbol{x}_1 = (-1, 0)$, $\boldsymbol{x}_2 = (1, 0)$, and $\boldsymbol{x}_3 = (1, \sqrt{2})$. The distance $l_{ij}(t)$ between the ith and jth vortices satisfies (for $i, j = 1, 2, 3$; $i \neq j$)

$$\frac{d}{dt} l_{ij}(t)^2 = \frac{2}{\pi} A \kappa_k \left(\frac{1}{l_{jk}^2} - \frac{1}{l_{ki}^2}\right),$$

where A denotes the area of the triangle and (i, j, k) are cyclic indices. Actually, we can deduce

$$\frac{d}{dt} l_{ij}(t)^2 = -\frac{1}{3\sqrt{2}\pi} l_{ij}(0),$$

from which we find

$$l_{ij}(t)^2 = l_{ij}(0)^2 \sqrt{1 - \frac{t}{3\sqrt{2}\pi}}.$$

This shows a collapse at $t = 3\sqrt{2}\pi$.

When the vortex strength and initial locations differ from the above, we set $\kappa_k = \alpha \kappa'_k$ and $l_{ij} = \beta l'_{ij}$ and write

$$\beta^2 \frac{d}{dt} (l'_{ij})^2 = \alpha \frac{2}{\pi} A' \kappa'_k \left(\frac{1}{(l'_{jk})^2} - \frac{1}{(l'_{ki})^2}\right)$$

or

$$\frac{d}{dt'} (l'_{ij})^2 = \frac{2}{\pi} A' \kappa'_k \left(\frac{1}{(l'_{jk})^2} - \frac{1}{(l'_{ki})^2}\right),$$

where $t' = \frac{\alpha}{\beta^2} t$.

[1] J. Jiménez and P. Moin, The minimal flow unit in near-wall turbulence, J. Fluid Mech. **225**, 213 (1991).
[2] M. Meldi and P. Sagaut, Turbulence in a box: Quantification of large-scale resolution effects in isotropic turbulence free decay, J. Fluid Mech. **818**, 697 (2017).
[3] K. Schneider and M. Farge, Final states of decaying 2D turbulence in bounded domains: Influence of the geometry, Physica D **237**, 2228 (2008).
[4] J. C. Robinson, Using periodic boundary conditions to approximate the Navier-Stokes equations on $\mathbb{R}^3$ and the transfer of regularity, Nonlinearity **34**, 7683 (2021).
[5] E. Segre and S. Kida, Late states of incompressible 2D decaying vorticity fields, Fluid Dyn. Res. **23**, 89 (1998).
[6] G. K. Batchelor, Computation of the energy spectrum in homogeneous two-dimensional turbulence, Phys. Fluids **12**, II-233 (1969).
[7] R. H. Kraichnan, Inertial ranges in two-dimensional turbulence, Phys. Fluids **10**, 1417 (1967).
[8] C. E. Leith, Diffusion approximation for two-dimensional turbulence, Phys. Fluids **11**, 671 (1968).
[9] G. Boffetta and R. E. Ecke, Two-dimensional turbulence, Annu. Rev. Fluid Mech. **44**, 427 (2012).
[10] A. Bracco, J. C. McWilliams, G. Murante, A. Provenzale and J. B. Weiss, Revisiting freely decaying two-dimensional turbulence at millennial resolution, Phys. Fluids **12**, 2931 (2000).
[11] E. Lindborg and A. Vallgren, Testing Batchelor's similarity hypotheses for decaying two-dimensional turbulence, Phys. Fluids **22**, 091704 (2010).
[12] S. Fox and P. A. Davidson, Freely decaying two-dimensional turbulence, J. Fluid Mech. **659**, 351 (2010).
[13] P. L. Sulem and U. Frisch, Bounds on energy flux for finite energy turbulence, J. Fluid Mech. **72**, 417 (1975).
[14] A. Pouquet, On two-dimensional magnetohydrodynamic turbulence, J. Fluid Mech. **88**, 1 (1978).
[15] H. A. Rose and P. L. Sulem, Fully developed turbulence and statistical mechanics, J. Phys. (Paris) **39**, 441 (1978).
[16] P. G. Saffman, On the spectrum and decay of random two-dimensional vorticity distributions at large Reynolds number, Stud. Appl. Math. **50**, 377 (1971).
[17] A. D. Gilbert, Spiral structures and spectra in two-dimensional turbulence, J. Fluid Mech. **193**, 475 (1988).
[18] G. L. Eyink, Dissipative anomalies in singular Euler flows, Physica D **237**, 1956 (2008).
[19] M. C. Lopes Filho, A. L. Mazzucato, and H. J. Nussenzveig Lopes, Weak solutions, renormalized solutions and enstrophy defects in 2D turbulence, Arch. Rat. Mech. Anal. **179**, 353 (2006).
[20] G. L. Eyink, Dissipation in turbulent solutions of 2D Euler equations, Nonlinearity **14**, 787 (2001).
[21] C. V. Tran and D. G. Dritschel, Vanishing enstrophy dissipation in two-dimensional Navier-Stokes turbulence in the inviscid limit, J. Fluid Mech. **559**, 107 (2006).
[22] D. Chae and P. Dubovskii, Functional and measure-valued solutions of the Euler equations for flows of incompressible fluids, Arch. Ration. Mech. Anal. **129**, 385 (1995).
[23] T. Gotoda and T. Sakajo, Distributional enstrophy dissipation via the collapse of three point vortices, J. Nonlin. Sci. **26**, 1525 (2016).
[24] J. P. Boyd, *Chebyshev and Fourier Spectral Methods* (Dover, New York, 2001).
[25] H. J. H. Clercx, A spectral solver for the Navier-Stokes equations in the velocity-vorticity formulation for flows with two nonperiodic directions, J. Comput. Phys. **137**, 186 (1997)
[26] N. Nguyen van yen, M. Waidmann, R. Klein, M. Farge, and K. Schneider, Energy dissipation caused by boundary layer instability at vanishing viscosity, J. Fluid Mech. **849**, 676 (2018).
[27] A. Cheskidov, P. Constantin, S. Friedlander, and R. Shvydkoy, Energy conservation and Onsager's conjecture for the Euler equations, Nonlinearity **21**, 1233 (2008).
[28] C. Bardos and U. Frisch, in *Turbulence and Navier Stokes Equations*, edited by R. Temam, Lecture Notes in Mathematics Vol. 565 (Springer, Berlin, 1975), pp. 1–13.
[29] Y. Giga and T. Kambe, Large time behavior of the vorticity of two-dimensional viscous flow and its application to vortex formation, Commun. Math. Phys. **117**, 549 (1988).
[30] M. Giga, Y. Giga, and J. Saal, *Nonlinear Partial Differential Equations: Asymptotic Behavior of Solutions and Self-Similar Solutions* (Springer, Berlin, 2010).
[31] Y. G. E. Sinai, Navier Stokes systems with periodic boundary conditions, Regul. Chaotic Dyn. **4**, 3 (1999).

[32] M. Oliver and E. S. Titi, Remark on the rate of decay of higher order derivatives for solutions to the Navier-Stokes equations in $\mathbb{R}^n$, J. Funct. Anal. **172**, 1 (2000).
[33] H. Kozono and T. Ogawa, Two-dimensional Navier-Stokes flow in unbounded domains, Math. Ann. **297**, 1 (1993).
[34] H. Kozono and T. Ogawa, Decay properties of strong solutions for the Navier-Stokes equations in two-dimensional unbounded domains, Arch. Ration. Mech. Anal. **122**, 1 (1993).
[35] N. K.-R. Kevlahan and M. Farge, Vorticity filaments in two-dimensional turbulence: Creation, stability and effect, J. Fluid Mech. **346**, 49 (1997).
[36] C. Marchioro and M. Pulvirenti, *Mathematical Theory of Incompressible Nonviscous Fluids* (Springer, Berlin, 2012).
[37] P. K. Newton, *The N-Vortex Problem: Analytical Techniques* (Springer, Berlin, 2001).
[38] K. A. O'Neil, Collapse of point vortex lattices, Physica D **37**, 531 (1989).
[39] M. A. Stremler and H. Aref, Motion of three point vortices in a periodic parallelogram, J. Fluid Mech. **392**, 101 (1999).
[40] M. Taylor, *Partial Differential Equations* (Springer, Berlin, 1996).
[41] R. Bellman, *A Brief Introduction to Theta Functions* (Dover, New York, 2013).
[42] *NIST Handbook of Mathematical Functions*, edited by F. W. J. Olver, D. W. Lozier, R. F. Boisvert, and C. W. Clark (Cambridge University Press, Cambridge, 2010).